Lawrence Berkeley National Laboratory

Title
Non-Bloch nature of alloy states in a conventional semiconductor alloy - GaxIn1-xP as an example

Permalink
https://escholarship.org/uc/item/6zh67152

Author
Zhang, Yong

Publication Date
2008-08-11

Non-Bloch nature of alloy states in a conventional semiconductor alloy - $Ga_xIn_{1-x}P$ as an example

Yong Zhang,*[1] A. Mascarenhas,[1] and L.-W. Wang[2]

[1]*National Renewable Energy Laboratory, 1617 Cole Blvd. Golden, CO 80401*

[2]Lawrence Berkeley National Laboratory, Berkeley, CA 94720

Abstract

Contrary to the conventional wisdom, electronic states in a "well behaved" semiconductor alloy such as $Ga_xIn_{1-x}P$ may drastically deviate from a Bloch state, which can be true even for band edge states if they are derived from degenerate critical points. For $Ga_xIn_{1-x}P$ in the entire composition range, **k**-space spectral analyses are performed for the important critical points, revealing the significance of the (near) resonant inter-and intra- valley scatterings of the fluctuation potential in the alloy. The non-trivial impications of such scatterings on the transport and strain effect are discussed.

* yong_zhang@nrel.gov

An electronic state in a conventional semiconductor alloy A_xB_{1-x} is often described in the same way as in a pure semiconductor, i.e., using a well defined **k** vector in the reduced Brillouin zone (BZ) within the framework of the "virtual crystal approximation (VCA)".[1, 2] The conventional wisdom seems to suggest that the effect of disorder can be viewed as an energy shift from the VCA value plus a spectral broadening (at least for states near the band edge).[3, 4] Indeed, it has been verified theoretically that a fundamental band edge state (either the conduction band minimum, CBM, or valence band maximum, VBM) does contain more than 90% of one particular **k** component of the BZ.[5] Therefore, it appears reasonable to classify the alloy state according to the Bloch state symmetry ("majority representation"),[5] with the understanding that the deviation from the VCA does make an alloy somewhat different from a pure semiconductor in certain important aspects. Among them, are the zero-phonon emission and absorption at an indirect band gap,[6], a reduction in carrier mobility,[7] and various statistical effects such as the linewidth broadening in an optical transition.[8] However, it is not clear to what extent quantitatively the VCA picture remains useful for the global electronic structure of an alloy, i.e., including electronic states beyond the band edge (e.g., high lying critical points), and it has not been realized that there are subtle but important effects for the degenerate band edge states although at the first glance they seem to obey the "majority representation".[5] We now find that in a conventional alloy a large number of alloy states are surprisingly "non-Bloch" or it is not always appropriate to associate an alloy state with a well defined **k** point, and there are strong inter-valley scatterings among the degenerate critical points of the VCA. These

findings should have significant impacts on the understanding of optical and transport properties of the alloy in general.

We have choosen the alloy system $Ga_xIn_{1-x}P$ for this study. This system has been shown to exhibit zero-phonon absorption and emission even in the indirect band-gap region with small amount of In ($< 10\%$).[9, 10] It is also well known to exhibit spontaneous ordering when grown by MOCVD.[11] Besides being widely used in HBT's for telecommunications, the alloy with x ~ 0.5 is a key component in a lattice-matched three-junction solar cell (with GaAs and Ge) that has yielded a record efficiency of 34.7%.[12] We have previously investigated the electronic structure near the fundamental bandgap for x ~ 0.5 as a function of order parameter, using an empirical pseudopotential method (EPM), and achieved remarkably excellent agreement between experiment and theory.[13, 14] Recently, $Ga_xIn_{1-x}P$ alloys with either x < 0.5 or x > 0.5 have been used as active layers in novel cell structures, which have yielded a new record efficiency of 40.7%,[12] and have great potential for further improvement. Motivated by the general interest in the basic physics of semiconductor alloys and the practical need for better understanding this important alloy system, we now extend the electronic structure calculation not only to the whole x range but also to higher critical points.

The EPM used in the previous and this work consists of two significant improvements over the conventional one to better account for the local atomic environment in the alloy system of the two binaries:[15] (1) the pseudopotential for the common anion (P) is taken as a weighted average according to the number of Ga and In atoms on the four nearest-neighbor cation sites; (2) the pseudopotential includes a correction term that allows the pseudopotential to be adjusted for the local atomic

distance which is usually different from that in the bulk. Empirical pseudopotentials for bulk GaP and InP are obtained separately by fitting to the experimentally determined or theoretically calculated electronic properties at their equilibrium conditions. These properties include energies, deformation potentials, effective masses at different critical points, and valence band offsets. The pseudopotentials can reproduce very well not only the binary band structures but also the alloy band structure at x ~ 0.5 with varying degree of ordering.[13, 14] The pseudopotential also contains a non-local spin-orbit interaction component. A plane-wave basis is used to expand the electronic wavefunction, with a kinetic-energy cutoff of 7 Ry.

A supercell approach is used to model the random alloy. For future convenience in studying the so-called CuPt ordering that often occurs in this alloy system along the [111] direction, an orthorhombic supercell is built with three cell vectors $\mathbf{a}_1$, $\mathbf{a}_2$ and $\mathbf{a}_3$ along the $x' \sim [11\overline{2}]$, $y' \sim [\overline{1}10]$ and $z' \sim [111]$ direction of the zinc-blende (ZB) crystal, respectively.[13] The lattice constant $a(x)$ is assumed to obey Vegard's rule with $a_{\mathrm{GaP}} = 5.447$ Å and $a_{\mathrm{InP}} = 5.8658$ Å. A supercell containing 27648 atoms, with $a_1 = 12\sqrt{3/2}\,a$, $a_2 = 12\sqrt{2}\,a$ and $a_3 = 8\sqrt{3}\,a$, is used for most analyses, which ensures the bandgap converging to within few meV.[13] Similar accuracy has been achieved for an $Al_xGa_{1-x}As$ alloy modeled by a tight-binding approach with the same order of supercell size.[16] Initially all atoms in the supercell occupy the ZB sites, but are relaxed to minimize the strain energy, using the valence force field method.[17] To solve the Schrodinger equation for the large systems involved, a folded spectrum method is used,[18] which allows to solve for only the states near the band edge within an energy range of interest (e.g., including Γ, L, and X point). To obtain and analyze eigenstates far away from the

band edge, a smaller supercell of 3456 atoms (a factor of 2 reduction in each dimension) is used. For such cases, a "representative" configuration that closely matches the average bandgap, the VBM and CBM energy from 50 different configurations is selected. The averaged bandgap of the smaller supercell is in fact very close to that of the larger one (within 1-2 meV).

Let $\varphi_i(\mathbf{r})$ be the eigenfunction of an alloy eigenstate with energy E, it can be expanded in a complete set of Bloch states $[\phi_n(\mathbf{k},\mathbf{r})]$ with band index n and wavevector $\mathbf{k}$ defined in the ZB BZ. A natural choice for $[\phi_n(\mathbf{k},\mathbf{r})]$ would be the VCA solutions of the same system. The degree of how the alloy state resembles the Bloch state can be quantitatively described by a $\mathbf{k}$-space projection function[5]

$$P_i(k) = \sum_n \left| < \varphi_i(r) \mid \phi_n(k,r) > \right|^2 .$$
(1)

If $\varphi_i(\mathbf{r})$ is dominated by one component $\mathbf{k}_0$ with a limiting value $P_i(\mathbf{k}_0) = 1$, we may consider this state to be primarily derived from the $\mathbf{k}_0$ Bloch state of the virtual crystal, and the spectrum of $P_i(\mathbf{k})$ reveals how many other ($\mathbf{k} \neq \mathbf{k}_0$) Bloch states the $\mathbf{k}_0$ state are coupled to by the potential fluctuation. Alternatively, one can define a spectral function [3, 19]

$$A(k_0, E) = \sum_i P_i(k_0)\delta(E - E_i) .$$
(2)

$A(\mathbf{k}_0,E)$ instead indicates to what extent the $\mathbf{k}_0$ Bloch state is mixed into other states of different energies. In the supercell approach, we calculate enough eigenstates of the supercell (at k = 0) to include all the folded states from the Γ, L, and X point of the ZB BZ, and evaluate $P_i(k)$ for each of them. The convergence of $P_i(\mathbf{k})$ with increasing the supercell size is somewhat slower than the energy levels, especially for those high lying

states. Whenever possible, we use the results of the 27648-atom supercells for both energy and $P_i(\mathbf{k})$. However, in a few cases, because of limitations in the computational resources, we have to use the results of 3456-atom supercell, and the $P_i(\mathbf{k})$ so obtained should be considered as the upper bound.

For the whole composition range $0 \leq x \leq 1$, Figure 1 shows the alloy energy levels derived from the three ZB critical points (Γ, L, and X) of the conduction band (CB) and from the ZB Γ point of the valence band (VB), with the corresponding $\mathbf{k}$-projection $P_i(\mathbf{k})$.

One of the surprising findings is that many alloy states within the VB and CB are in fact questionable to be viewed as Bloch-like states, even for as little as 10% deviation from the endpoints x = 0 or 1. The degree of alloy fluctuation induced $\mathbf{k}$-space mixing sensitively depends on the number of states available for coupling or roughly the density of states, if we take the VCA Bloch states as the zero order approximation. For the VB, there are two close by states with large and comparable Γ projections. The small splitting (0.4 - 2.2 meV) could be viewed as a residual effect deviating from the ZB structure. We thus define the VBM as the weighted average of the two states by their Γ projections. Fig.1(a) shows the x-dependence of VBM and its Γ component $P_{VBM}(\Gamma)$. Indeed, the VBM behavior is just what is expected from the standard understanding of the alloy: the "majority representation" holds with $P_{VBM}(\Gamma) > 0.84$, and the effect of the alloy fluctuation maximizes at x ~ 0.5, qualitatively following the x(1-x) rule. The situation for the CB is nevertheless much more complex. Fig.1(b) shows x-dependence for the energy levels and Fig.1(c) for the corresponding $\mathbf{k}$ projections. For x < 0.7, the CBM is primarily derived from the Γ state with $P_{CBM}(\Gamma)$ or $P_\Gamma > 0.80$, thus can indeed be viewed as Bloch-like. However, the other two critical points, the L- and X-like (the definitions are given

later) may contain significant contributions from other **k** points. Especially, for the X derived alloy state, the projection P_X drops to close to 0.1 at x = 0.5. Beyond x = 0.7, P_Γ dips even below 0.1 at x ~ 0.8, which makes it rather ambiguous to even called it Γ-like, although it does have the largest Γ component among the states within the expected energy range. The alloy fluctuation is found to induce significant splittings among the 4-fold or 3-fold degenerate L or X point. In Fig1(b), the energy level of the L-like state E_L is defined as the weighted average of the 4 alloy states with the largest L projections $P_i(L) = \sum_j^4 P_i(L_j)$, and the average L component P_L is defined by $\sum_j^4 |E_i - E_L|^{-1} P_i(L) / \sum_j^4 |E_i - E_L|^{-1}$. The X point energy E_X and the average X component P_X are defined in a similar manner. The strong variations shown in Fig.1(c) for the **k** projections can be understood qualitatively by following the evolution of the overall CB structure with varying x. For instance, for the X-like state starting from x = 0, being a rather high lying state, there are a large number of nearly degenerate VCA states that may be coupled by the potential fluctuation, therefore, the decrease of P_X with initial increase in x (0 < x < 0.5) is much faster than that of P_Γ when the Γ-like is the band edge state. A similar effect has been observed in highly mismatched alloy $GaP_{1-x}N_x$ at even lower composition (x ~ 0.1%).[20] Upon further increasing x (0.5 < x < 0.75), the X-like states become substantially closer to the band edge, which leads to a reduction of the states available for coupling, and together with reducing the alloy fluctuation, P_X increases. Beyond x > 0.75 after X-like state turns into the CBM, P_X becomes greater than 85%. Concomitantly, the Γ-like state becomes resonant, and thus P_Γ decreases rapidly at first but recovers as x further approaching 1.

Figure 2 shows A(k_0,E) for alloy states near the CBM with $\mathbf{k_0} = \mathbf{k_\Gamma}$, $\mathbf{k_L}$, and $\mathbf{k_X}$ and for x = 0.25, 0.50, and 0.80. At x = 0.25 and 0.50, the high-lying X-like state shows strong mixing with nearby states; at x = 0.80, although quite close to the band edge, the resonant Γ-like state E_Γ, the one with the largest P_Γ, couples with many states below and above it. Although the state identified as Γ-like only has $P_\Gamma \approx 0.092$, the sum of the Γ projections for all the states below equals 0.445, and for all the states above should be 0.463, implied by the sum rule, which explains why this state still falls on the smooth curve for the Γ-like state in Fig.1(b). Despite the CBM being X-like at x = 0.80, the coupling with the Γ-like state does yield a finite Γ component ∼ 0.5 %, which is sufficient to produce the zero-phonon absorption or emission at the X-like fundamental bandgap.[9, 10] It is worth mentioning that because of the high degeneracy of the VB, it is found that at x = 0.50 the spin-orbit split off band has only ∼ 45% of the Γ component, even though being merely ∼ 100 meV below the VBM, which might be reflected in the weakness of the spin-orbit feature in absorption and modulation spectra for samples with x ∼ 0.5.[21]

Another important finding is that there is a strong inter-valley mixing among the degenerate critical points $\mathbf{k_0}$'s in the VCA, even in the case they are the CBM and have a high overall purity. Specifically, we consider the case x = 0.80 for which the CBM is X-like with $P_X > 0.9$. For each individual state of all the three split X-like state, $P_i(k_X)$ has nearly equal contribution, 0.3±0.2, from the three independent valleys (i.e., [100], [010], and [001]), by averaging 50 different 3456-atom configurations. The equal partition reveals the significance of the inter-valley scattering in an otherwise believed simple alloy, and the large fluctuation (the standard deviation) indicates the sensitivity of the intervalley scattering on the detail of the atomic configuration. Similar results are

obtained from a few 27648-atom supercells. The inter-valley scatterings are practically important if we further notice the fact that the energy spread of the each individual split state is larger than their splittings. There are two important implications: (1) on the macroscopic scale, the alloy band edge state is a uniform mixture of the three independent Bloch states associated with the three $\mathbf{k}_X$ points in the VCA picture, which is of significance for understanding certain alloy behaviors, such as the response to an uniaxial strain along an [001] type axis; (2) on the mesoscopic scale, the mixing is quite non-uniform, which is of significance for instance for the electron conductivity, if an alloy is viewed as a superposition of domains of different random configurations. It is reasonable to expect that the impact to the electron mobility could be more severe in the indirect-gap than in the direct-gap composition region because of the inter-valley scattering for the former, in addition to the commonly known mechanism that the indirect bandgap tends to have a larger effective mass. We further note that the inter-valley and intra-valley scattering have comparable strength among degenerate states, which means that they should be accounted for with approximately equal weights when an emperical formula[7, 22] is used to describe the carrier mobility in an alloy (e.g., the degeneracy factor $g = 3 + C_3^2 = 6$ for the indirect GaInP alloy).

Next we discuss the x-dependence of the VBM, three critical points of the CB, shown in Fig.1(b), and the relevant bandgaps, shown in Figure 3. The numerical results are fitted with the following well known equation:

$$E(x) = E(0) + [E(1) - E(0)]x - b(x)x(1 - x).$$

(3)

We have found that a bowing parameter in the form of $b(x) = b_0 + b_1 x$ can fit all the critical points very well. The fitting parameters are summarized in Table 1. The results for individual critical points can be used to obtain the natural band offsets between any two compositions. The CBM Γ to X crossing occurs at $x_{\Gamma-X} = 0.749$, which agrees well with reported values: 0.74 from optical measurements,[9, 23], ≥ 0.73 from a mobility measurement,[24] and 0.74 from a theoretical analysis.[25] Two other crossing points, L to X and Γ to L (the energy moves from lower to higher), are found to be $x_{L-X} = 0.725$ and $x_{\Gamma-L} = 0.768$, respectively, both above the CBM. The current $x_{\Gamma-X}$ value is substantially more accurate than $x_{\Gamma-X} = 0.695$ of an early calculation that also gave significantly different values for $x_{L-X} = 0.571$ and $x_{\Gamma-L} = 0.783$.[2] More relevant to optical measurements are the bandgaps. A noticeable difference between $E_X(x)$ and $E_{gX}(x)$ is that while the former decreases monotonically from $x = 0$ to 1, the latter is nearly flat between $x = 0.75$ and 1, due to the contribution of the VBM bowing. Comparisons with experimental data are shown in Fig.3. Although the agreement is in general quite good, one should be aware that the accuracy of earlier experimental data could suffer from the uncertainty in the composition determination, and that the current calculation does not include the excitonic effect.

Captions

Figure 1. Calculated critical point energies and the corresponding **k**-space projections for $Ga_xIn_{1-x}P$ alloys. (a) for the valence band maximum and the **k**-space projection, (b) for the critical points of the conduction band, and (c) for the **k**-space projections of the conduction band critical points. Solid symbols represent the results from 27648-atom supercells, and open symbols from 3456-atom supercells. Solid lines are fitting curves, and dashed lines are guides to the eyes.

Figure 2. Spectral function $A(k_0,E)$ of $Ga_xIn_{1-x}P$ for critical points of $\mathbf{k_0} = \mathbf{k_\Gamma}$, $\mathbf{k_L}$, and $\mathbf{k_X}$. Solid and open symbols are the results using 27648-atom and 3456-atom supercells, respectively. Energy references are the conduction band minimums in Fig.1(b).

Figure 3. Calculated bandgaps of $Ga_xIn_{1-x}P$ alloys, compared with experimental data. Solid symbols and lines are calculated results and fitting curves. Dashed line from Ref.[26]for Eg_Γ (at 77 K), dotted line from Ref.[9] for E_{gX}(21 K), open circles from Ref.[27] (10 K), and open triangle from Ref.[21] (5 K).

Table 1. Fitting parameters for used with Eq.(3) (in eV).

References

[1]   L. Nordheim, Ann. Phys. (Leipzig) **9**, 607 (1931).

[2]   A. B. Chen, and A. Sher, Semiconductor alloys, physics and materials engineering (1995).

[3]   K. C. Hass, H. Ehrenreich, and B. Velický, Phys. Rev. B **27**, 1088 (1983).

[4]   R. J. Lempert, K. C. Hass, and H. Ehrenreich, Phys. Rev. B **36**, 1111 (1987).

[5]   L. W. Wang *et al.*, Phys. Rev. Lett. **80**, 4725 (1998).

[6]   A. N. Pikhtin, Fiz. Tekh. Poluprovodn. **11**, 245 (1977).

[7]   V. Venkataraman, C. W. Liu, and J. C. Sturm, Appl. Phys. Lett. **63**, 2795 (1993).

[8]   K. K. Bajaj, Mater. Sci. Eng. R Rep. **R34**, 59 (2001).

[9]   J. Donecker, and J. Kluge, Phys. Status Solidi B **71**, K1 (1975).

[10]   A. N. Pikhtin, and A. V. Solomonov, Fiz. Tekh. Poluprovodn. **11**, 329 (1977).

[11]   A. Mascarenhas, *Spontaneous Ordering in Semiconductor Alloys* (Kluwer Academic/Plenum Publishers, New York, 2002).

[12]   M. A. Green *et al.*, Prog. Photovolt., Res. Appl. **15**, 425 (2007).

[13]   Y. Zhang, A. Mascarenhas, and L. W. Wang, Phys. Rev. B **63**, R201312 (2001).

[14]   Y. Zhang, A. Mascarenhas, and L. W. Wang, Appl. Phys. Lett. **80**, 3111 (2002).

[15]   L.-W. Wang, J. Kim, and A. Zunger, Phys. Rev. B **59**, 5678 (1999).

[16]   F. Oyafuso *et al.*, Journal of Computational Electronics **1**, 317 (2002).

[17]   P. Keating, Physical Review **145**, 637 (1966).

[18]   L. W. Wang, and A. Zunger, J. Chem. Phys. **100**, 2394 (1994).

[19]   L. C. Davis, Phys. Rev. B **28**, 6961 (1983).

[20]   Y. Zhang, A. Mascarenhas, and L.-W. Wang, Phys. Rev. B **74**, 041201(R) (2006).

[21]   B. Fluegel *et al.*, Phys. Rev. B **55**, 13647 (1997).

[22]   S. Krishnamurthy, A. Sher, and A.-B. Chen, Appl. Phys. Lett. **47**, 160 (1985).

[23]   A. Onton, and R. J. Chicotka, Phys. Rev. B **4**, 1847 (1971).

[24]   H. M. Macksey *et al.*, J. Appl. Phys. **44**, 1333 (1973).

[25]   M. Altarell, Solid State Commun. **15**, 1607 (1974).

[26]   H. Lange, J. Donecker, and H. Friedrich, Phys. Status Solidi B **73**, 633 (1976).

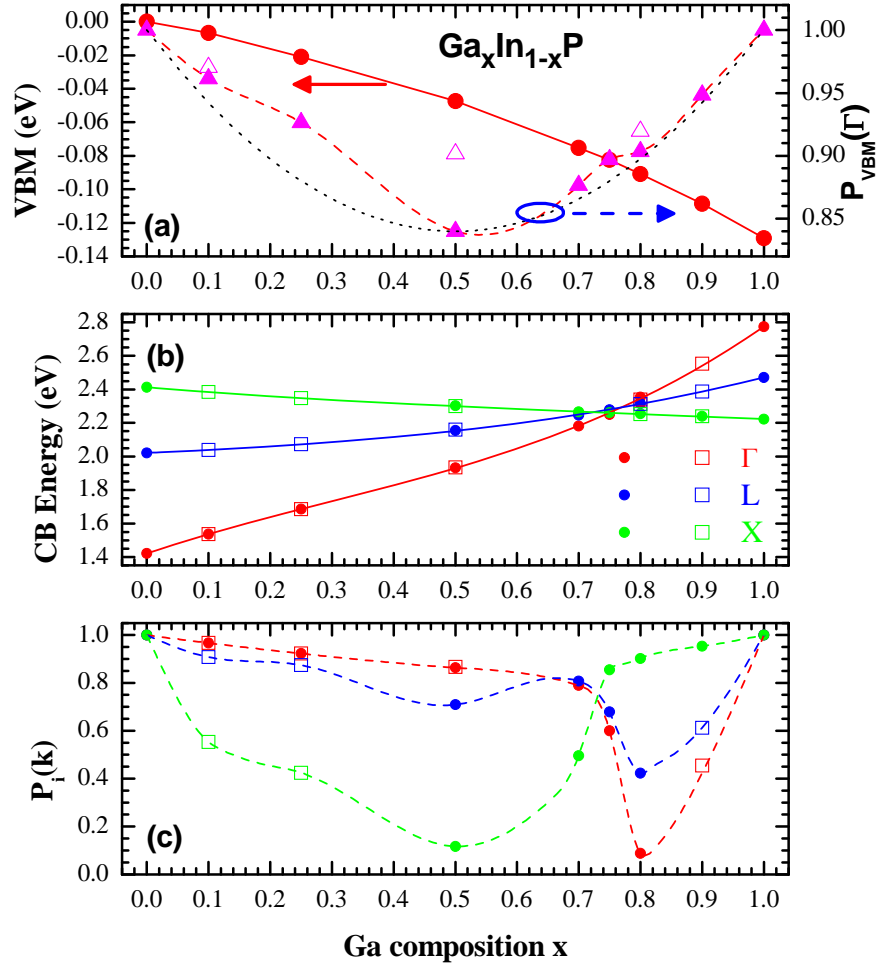[27]   P. Merle *et al.*, Phys. Rev. B **15**, 2032 (1977).

Figure 1. Calculated critical point energies and the corresponding **k**-space projections for $Ga_xIn_{1-x}P$ alloys. (a) for the valence band maximum and the **k**-space projection, (b) for the critical points of the conduction band, and (c) for the **k**-space projections of the conduction band critical points. Solid symbols represent the results from 27648-atom supercells, and open symbols from 3456-atom supercells. Solid lines are fitting curves, and dashed lines are guides to the eyes.
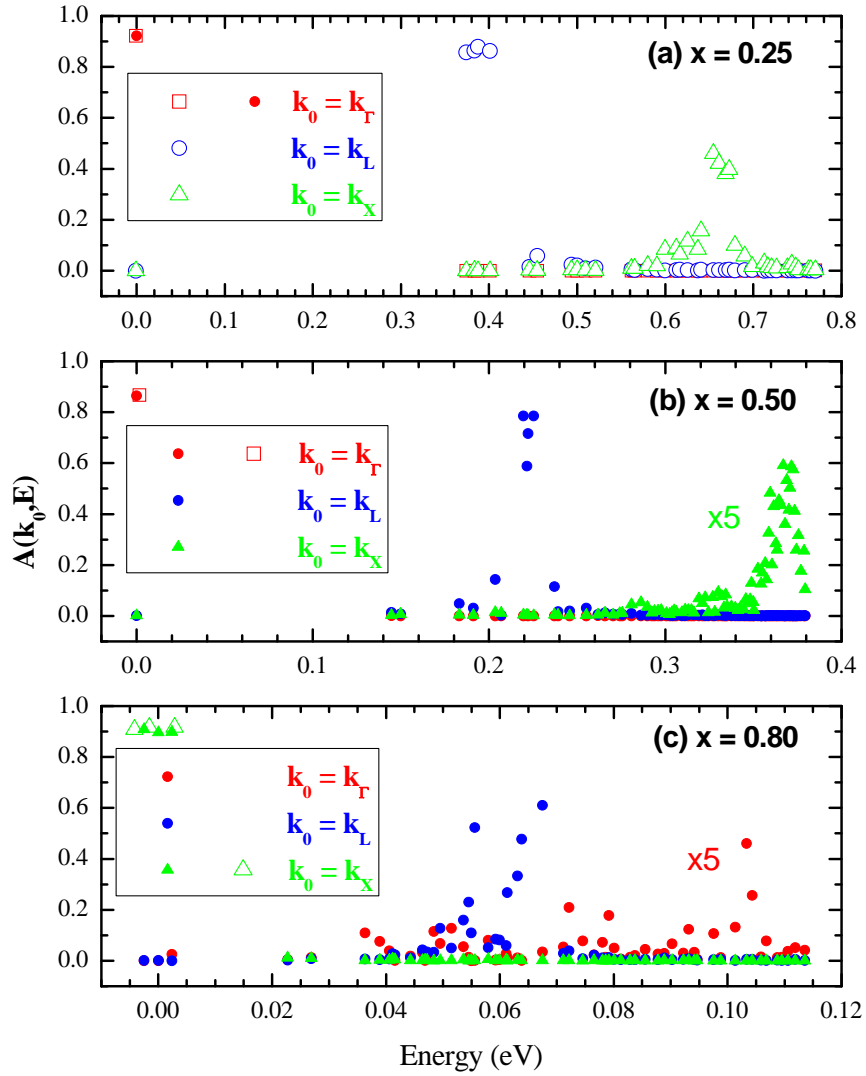
Figure 2. Spectral function A(k₀,E) of $Ga_xIn_{1-x}P$ for critical points of $\mathbf{k_0} = \mathbf{k}_\Gamma$, $\mathbf{k}_L$, and $\mathbf{k}_X$. Solid and open symbols are the results using 27648-atom and 3456-atom supercells, respectively. Energy references are the conduction band minimums in Fig.1(b).
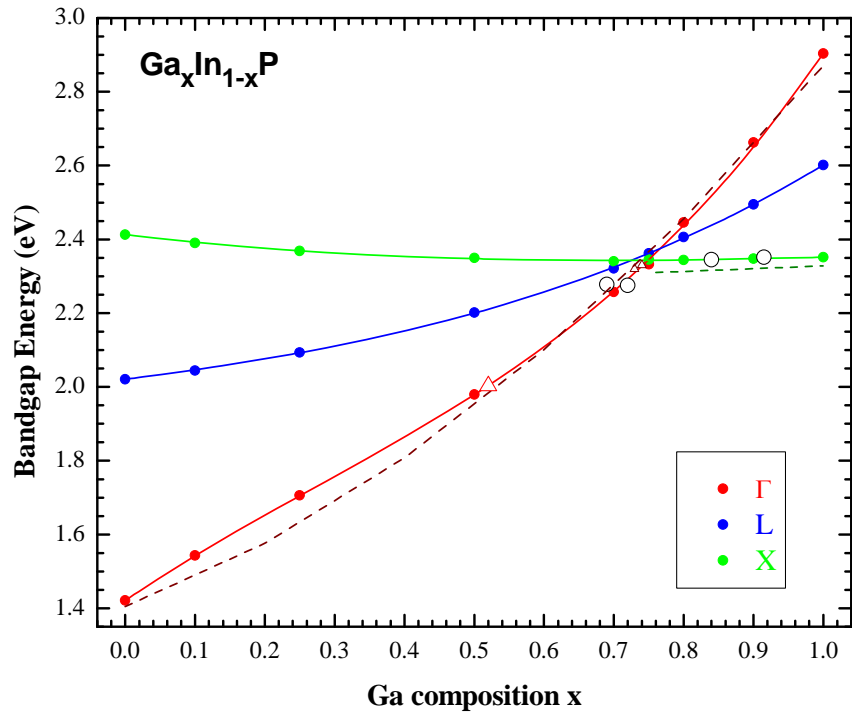
Figure 3. Calculated bandgaps of $Ga_xIn_{1-x}P$ alloys, compared with experimental data. Solid symbols and lines are calculated results and fitting curves. Dashed line from Ref.[26]for Eg_Γ (at 77 K), dotted line from Ref.[9] for E_{gX}(21 K), open circles from Ref.[27] (10 K), and open triangle from Ref.[21] (5 K).

Table 1. Fitting parameters for used with Eq.(3) (in eV).

	E(0)	E(1)-E(0)	b_0	b_1
$E_{CB\Gamma}$	1.421	1.353	0.139	1.051
E_{CBL}	2.021	0.451	0.282	0.187
E_{CBX}	2.412	-0.190	0.109	-0.079
E_{VBM}	0	-0.129	-0.056	-0.026
$E_{g\Gamma}$	1.421	1.482	0.195	1.078
E_{gL}	2.021	0.580	0.338	0.213
E_{gX}	2.412	-0.060	0.165	-0.052